Structural basis for extracellular interactions between calcitonin receptor-like receptor and receptor activity-modifying protein 2 for adrenomedullin-specific binding

Seisuke Kusano,[1] Mutsuko Kukimoto-Niino,[1] Nobumasa Hino,[1] Noboru Ohsawa,[1] Ken-ichi Okuda,[1] Kensaku Sakamoto,[1] Mikako Shirouzu,[1] Takayuki Shindo,[2] and Shigeyuki Yokoyama[1,3]*

[1]RIKEN Systems and Structural Biology Center, 1-7-22 Suehiro-cho, Tsurumi-ku, Yokohama 230-0045, Japan

[2]Department of Organ Regeneration, Graduate School of Medicine, Shinshu University, Matsumoto, Nagano 390-8621, Japan

[3]Laboratory of Structural Biology, Department of Biophysics and Biochemistry, Graduate School of Science, The University of Tokyo, Bunkyo-ku, Tokyo 113-0033, Japan

Received 2 September 2011; Accepted 10 November 2011
DOI: 10.1002/pro.2003
Published online 18 November 2011 proteinscience.org

Abstract: The calcitonin receptor-like receptor (CRLR), a class B GPCR, forms a heterodimer with receptor activity-modifying protein 2 (RAMP2), and serves as the adrenomedullin (AM) receptor to control neovascularization, while CRLR and RAMP1 form the calcitonin gene-related peptide (CGRP) receptor. Here, we report the crystal structures of the RAMP2 extracellular domain alone and in the complex with the CRLR extracellular domain. The CRLR–RAMP2 complex exhibits several intermolecular interactions that were not observed in the previously reported CRLR–RAMP1 complex, and thus the shape of the putative ligand-binding pocket of CRLR–RAMP2 is distinct from that of CRLR–RAMP1. The CRLR–RAMP2 interactions were confirmed for the full-length proteins on the cell surface by site-specific photo-crosslinking. Mutagenesis revealed that AM binding requires RAMP2 residues that are not conserved in RAMP1. Therefore, the differences in both the shapes and the key residues of the binding pocket are essential for the ligand specificity.

Keywords: G protein coupled receptors (GPCR); adrenomedullin (AM); calcitonin receptor-like receptor (CRLR); receptor activity-modifying protein (RAMP); neovascularization

Introduction

Adrenomedullin (AM), consisting of 52 amino acid residues, belongs to the calcitonin family of peptides, including calcitonin (CT), calcitonin gene-related peptide (CGRP), and amylin (AMY). AM was isolated from a human adrenal pheochromocytoma, as a novel hypotensive peptide with strong vasodilatation activity.[1] AM is produced by vascular smooth muscle cells and endothelial cells. By analyzing AM knockout mice, we demonstrated that AM is necessary for the stabilization of vascular integrity.[2] AM appears to have a variety of functions, including

Additional Supporting Information may be found in the online version of this article.

Grant sponsors: RIKEN Structural Genomics/Proteomics Initiative (RSGI), the National Project on Protein Structural and Functional Analyses and the Targeted Proteins Research Program (TPRP), the Ministry of Education, Culture, Sports, Science and Technology (MEXT) of Japan

*Correspondence to: Shigeyuki Yokoyama, RIKEN Systems and Structural Biology Center, 1-7-22 Suehiro-cho, Tsurumi-ku, Yokohama 230-0045, Japan. E-mail: yokoyama@riken.jp and yokoyama@biochem.s.u-okyo.ac.jp

Published by Wiley-Blackwell. © 2011 The Protein Society

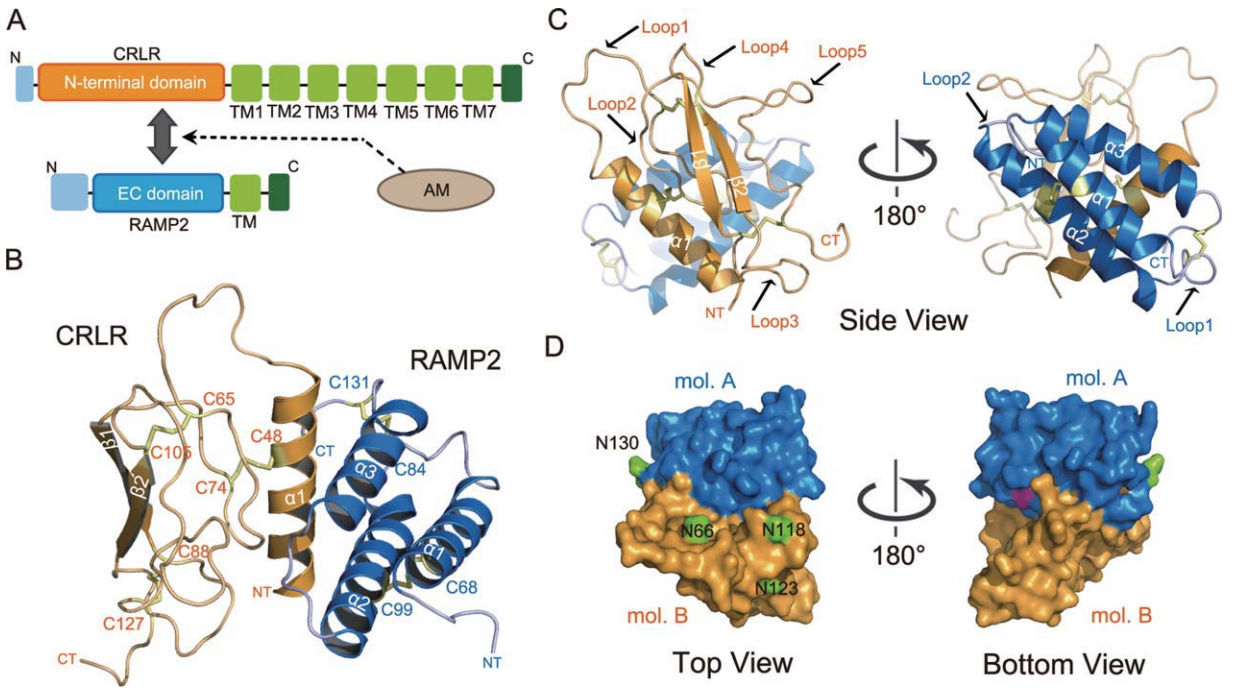

Figure 1. Overall complex structure of the human CRLR–RAMP2 ECDs. A: Domain organizations of CRLR and RAMP2. B: Cartoon representation of the crystal structure of the human CRLR–RAMP2 complex. CRLR and RAMP2 are colored orange and blue, respectively. For each protein, α helices and β strands are numbered sequentially. Disulfide bonds are represented as yellow stick models. C: Side views of the CRLR–RAMP2 complex structure, showing the loop positions of each protein. The two views are related by a 180° rotation about the vertical axis. D: Molecular surface representation of the CRLR–RAMP2 complex, viewed from the top and bottom. The glycosylation sites of each protein are colored green.

neovascularization, bronchodilatation, hormone secretion regulation, neurotransmission, cell growth regulation, apoptosis inhibition, antimicrobial activity, and others, in broad areas of the human body.[3–5] Therefore, AM is generally recognized as a potential therapeutic agent for the treatment of chronic diseases.[6,7]

The AM receptor consists of calcitonin receptor-like receptor (CRLR) and receptor activity-modifying protein 2 (RAMP2), with 1:1 stoichiometry [Fig. 1(A)].[8] CRLR belongs to the class B family of seven transmembrane-spanning G-protein coupled receptors (GPCRs), while RAMP2 is an accessory protein with a single transmembrane-spanning region. The class B GPCR family comprises 15 members, including calcitonin receptor (CTR) and CRLR, which are characterized by their relatively large and unique 100–160 residue N-terminal extracellular domains (ECDs, also known as ectodomains), containing three conserved disulfide bonds and the canonical seven transmembrane helix (7TM) motif.[9] These GPCRs utilize their ECDs to recognize polypeptide hormones,[10] including parathyroid hormone (PTH),[11] glucagon-like peptide (GLP),[12] gastric inhibitory peptide (GIP),[13] CT, CGRP, and AM.

RAMP2 facilitates the trafficking of CRLR from an intracellular compartment to the cell surface, and therefore is required for functional receptor formation.[8] The three RAMP isoforms (RAMP1–3) share less than 30% sequence identity with one another, and exhibit different tissue distributions.[8,14] All of them bind CRLR, and confer different specificities for peptide ligands on CRLR.[15] For example, the heterodimer consisting of CRLR and RAMP1 is specific for CGRP, while the CRLR–RAMP2 and CRLR–RAMP3 heterodimers are specific for AM. All three human RAMPs share a common domain organization: the N-terminal ECD (about 91 residues for RAMP1 and RAMP3, and about 102 residues for human RAMP2), the single transmembrane (TM) domain (about 22 residues), and the C-terminal short intracellular region (about 9 residues). We previously reported the first structure of the RAMP1 extracellular domain by an X-ray crystallographic analysis.[16] Recently, the crystal structures of the CRLR–RAMP1 heterodimer (the CGRP receptor) with clinical receptor antagonists were determined.[17] However, the structural basis of the AM receptor activity remains elusive.

In the present study, we determined the crystal structures of the RAMP2 ECD alone at 2.0 Å, and complexed with the CRLR ECD at 2.6 Å. We confirmed that the ECD complex retains the AM-binding activity *in vitro*, and that the two full-length proteins interact with each other in the same manner *in vivo*. The putative ligand-binding pocket of the CRLR–RAMP2 complex adopts a different shape from that of the CRLR–RAMP1 complex, which may

Table I. *X-Ray Data Collection, Phasing and Refinement Statistics of CRLR–RAMP2*

	Complex Peak	Complex Edge	Complex Remote
Data collection			
Wavelength (Å)	0.9790	0.9793	0.9640
Resolution (Å)	50–2.6 (2.69–2.60)	50–2.6 (2.69–2.60)	50–2.6 (2.69–2.60)
Unique reflections	6157	6100	5956
Redundancy	11.2	10.9	10.3
Completeness (%)	99.1 (91.8)	97.7 (84.7)	95.6 (75.8)
I/σ (I)	20.3 (5.9)	21.1 (4.78)	18.3 (4.15)
R_{sym}[a] (%)	11.5 (25.2)	11.0 (26.0)	11.5 (27.1)
MAD analysis			
Resolution (Å)	2.8		
No. of sites	5		
FOM_{MAD}[b]	0.56		
$FOM_{RESOLVE}$[c]	0.76		
Refinement			
Resolution (Å)	40.6–2.6		
No. of reflections	6075		
No. of protein atoms	1463		
No. of water molecules	30		
R_{work} (%)	22.2		
R_{free} (%)[d]	28.2		
R.m.s.d. bond length (Å)	0.019		
R.m.s.d. bond angles (°)	1.7		
Ramachandran plot			
Most favored regions (%)	96.5		
Additional allowed regions (%)	3.5		
Generously allowed regions (%)	0.0		
Disallowed regions (%)	0.0		

All numbers in parentheses represent last outer shell statistics.
[a] $R_{sym}=\sum |I_{avg} - Ii|/\sum Ii$, where Ii is the observed intensity and I_{avg} is the average intensity.
[b] Figure of merit after SOLVE phasing.
[c] Figure of merit after RESOLVE.
[d] R_{free} is calculated for 10 % of randomly selected reflections excluded from refinement.

underlie the distinct ligand-binding specificities between the AM and CGRP receptors.

Results and Discussion

Structure determination

We prepared the ECDs of human CRLR (Glu23–Lys136) and RAMP2 (Gly56–Ser139) by refolding them separately and mixing them together, but these proteins were separated by size-exclusion chromatography (SEC). In contrast, when the CRLR and RAMP2 ECDs were co-refolded, the two proteins formed a stable complex at an equimolar ratio. The resulting complex between the CRLR and RAMP2 ECDs (referred to hereafter as the CRLR–RAMP2 complex) behaved as the CRLR–RAMP2 heterodimer at 0.5 mg/mL, whereas it further dimerized to the heterotetramer $(CRLR–RAMP2)_2$ at 5 mg/mL, as revealed by the SEC analysis (Supporting Information Fig. S1).

We determined the crystal structure of the CRLR–RAMP2 complex at 2.6 Å resolution by the multi-wavelength anomalous dispersion (MAD) method, using the crystal of the selenomethionine-labeled proteins. The crystallographic data are summarized in Table I. The crystal of the CRLR–RAMP2 complex belongs to the primitive tetragonal space group $P4_12_12$, with unit cell constants of $a = b = 55.4$ Å, $c = 119.4$ Å, and contains one heterodimer per asymmetric unit. The final model includes 79 amino acid residues of RAMP2, 97 amino acid residues of CRLR, and 30 water molecules in the asymmetric unit. The five residues (Gln135–Ser139) at the C-terminus of the RAMP2 construct were not included in the final model, due to their very weak electron densities. Similarly, the thirteen residues (Glu23–Gly35) at the N-terminus and the four residues (Glu133–Lys136) at the C-terminus of the CRLR construct were not included in the final model.

In parallel, we determined the crystal structure of the RAMP2 ECD alone, at 2.0 Å resolution, by the MAD method. The crystallographic data are summarized in Supporting Information Table S1. The RAMP2 crystal belongs to the primitive orthorhombic space group $P2_12_12_1$, with unit cell constants of $a = 59.6$ Å, $b = 89.7$ Å, $c = 92.0$ Å, and contains six RAMP2 molecules in the asymmetric unit. The final model includes 76 amino acid residues (Gln56–Ser134) of six RAMP2 chains, and 172 water molecules.

Overall structure of the CRLR–RAMP2 extracellular complex

The structure of the CRLR–RAMP2 complex is shown in Figure 1(B). Overall, CRLR and RAMP2

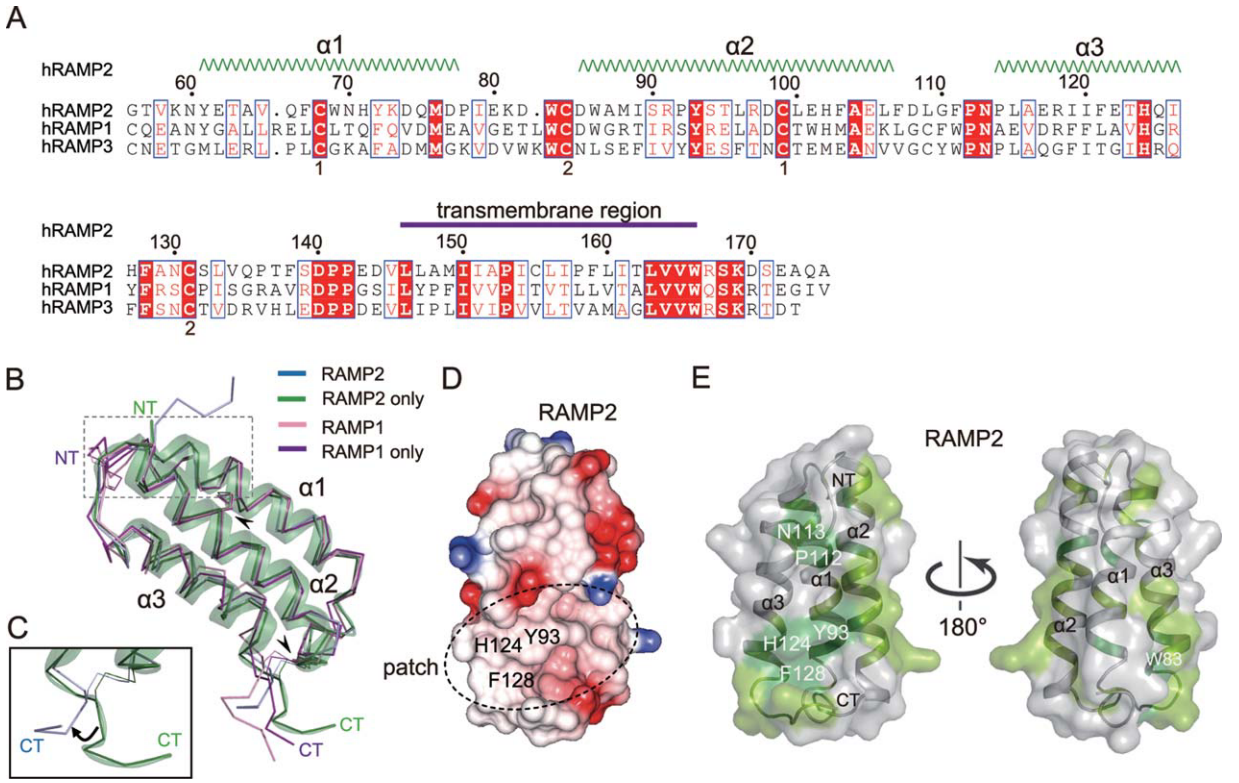

Figure 2. Sequence analysis and surface properties of RAMP2. A: Sequence alignment of human RAMPs, generated by ESPript[18] with CLUSTALW.[19] Identical and similar residues among the three RAMPs are represented with white and red characters, respectively, in blue boxes. The secondary structure of RAMP2 is shown above the sequences. Predicted signal peptide sequences for RAMP1 (residues 1–26), RAMP2 (1–35), and RAMP3 (1–23) are omitted from the alignment. The numbers below the sequences indicate the positions of cysteine residues involved in the formation of the first and second disulfide bonds (Cys68–Cys99, and Cys84–Cys131, respectively). The putative transmembrane region is represented by a violet bar. B: Superimposition of the Cα atoms of the RAMP2 and RAMP1 ECDs alone (green and purple, respectively) onto those complexed with CRLR (blue and pink). C: Close-up views of the C-terminal region of the RAMP2 extracellular domain, showing the structural differences observed upon CRLR binding. D: The electrostatic surface of RAMP2 at the CRLR–RAMP2 interface. Blue and red surfaces represent positive and negative potentials, respectively. The circle indicates the location of the hydrophobic patch, which forms the interface with CRLR. E: Residue conservation mapping on the surface of human RAMPs. Green and light green surfaces indicate the locations of identical and similar residues among human RAMPs, respectively, according to the sequence alignment in (A). The two views are related by a 180° rotation about the vertical axis.

form a heterodimer in a "side-by-side" orientation. The CRLR structure consists of an N-terminal α helix (α1), two anti-parallel β strands (β1 and 2), and five loop regions (loops 1–5), and is stabilized by three intramolecular disulfide bonds (Cys48–Cys74, Cys65–Cys105, and Cys88–Cys127) [Fig. 1(C)]. The RAMP2 structure adopts a three-helix bundle fold, consisting of α1–α3, which are connected by two loops (loops 1 and 2) [Fig. 1(C)]. In the CRLR–RAMP2 complex, the RAMP2 α2 and α3 helices interact with the CRLR α1 helix. The interface between CRLR and RAMP2 buries 924 Å^2, corresponding to 13.9% and 17.0% of the total surface areas of CRLR and RAMP2, respectively.

The overall architecture of the CRLR–RAMP2 complex is similar to that of the recently reported crystal structure of the CRLR–RAMP1 complex, or the CGRP receptor.[17] However, RAMP1 and RAMP2 share less than 30% sequence identity [Fig. 2(A)], and this difference in the amino acid residues results in significant variations in the heterodimer interface between the two structures, as described below.

RAMP2 possesses an N-glycosylation site (Asn130). The glycosylation of RAMP2 reportedly facilitates the trafficking of CRLR from the intracellular milieu to the cell surface.[20] In the present structure, the Asn130 residue in RAMP2 is located on one side of the heterodimer [Fig. 1(D)]. In contrast, CRLR has three N-glycosylation sites, which are all located on the upper side (i.e., the opposite side of the membrane surface). Among these three CRLR residues, the glycosylation of Asn123 is reportedly required for the trafficking of CRLR–RAMP2 to the cell surface.[21]

The CRLR–RAMP2 heterodimer is closely packed with the dyad symmetry-related heterodimer in the crystal [Supporting Information Fig. S2(A,B)]. This heterotetrameric structure is likely to correspond to the heterotetramer observed at high

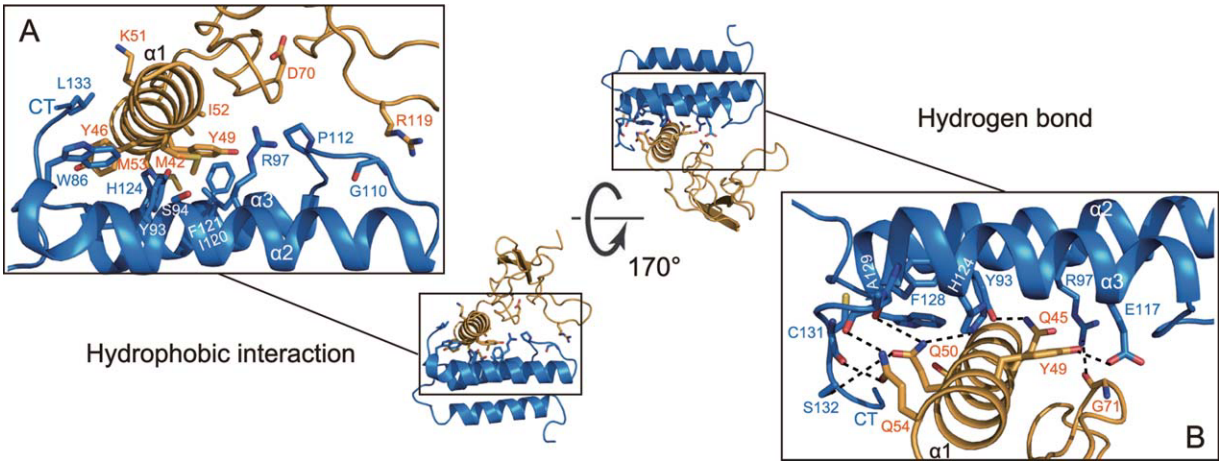

Figure 3. Interactions between CRLR and RAMP2. Two views of the interface, showing (A) hydrophobic interactions and (B) hydrogen bonds between RAMP2 (α2 and α3) and CRLR (α1). The two views are related by a 170° rotation about the horizontal axis. Interacting residues are displayed as stick models. Hydrogen bonds are indicated as dashed lines. Coloring schemes are the same as in Figure 1(B).

concentrations in solution [Supporting Information Fig. S1(A,C)]. The two CRLR–RAMP2 heterodimers interact in a "side-by-side" manner. The CRLR C-terminal tail and loop 5 interact with the RAMP2 N-terminal tail and loop 2, respectively [Supporting Information Fig. S2(C,D)]. These interactions bury 2111 Å^2 of surface area (10.3% of the total surface area). This interface does not involve any of the glycosylation sites of CRLR and RAMP2, but it buries the ligand-binding pocket of the CRLR–RAMP2 heterodimer (see subsequent sections).

Structure of RAMP2

In the three-helix bundle of RAMP2, α2 is aligned in an anti-parallel manner relative to α1 and α3. There are two disulfide bonds, Cys68–Cys99 and Cys84–Cys131, which connect α1 with α2 and loop 1 with the C-terminal tail, respectively. The mutations of C68A, C84A, C99A, and C131A in RAMP2 reportedly reduced the binding of AM with the AM receptor.[22] Therefore, the two disulfide bonds contribute to the stability of the RAMP2 structure.

A comparison of the present structure of RAMP2 alone with that of RAMP1, which we solved previously,[16] reveals that these folds are well conserved [Fig. 2(B)]. However, α1 is straight in the RAMP2 structure, whereas the corresponding helix of RAMP1 is kinked in the middle. In addition, the Cys27–Cys82 disulfide bond, which connects the RAMP1 N-terminus to loop 2, is absent in RAMP2.

The structures of RAMP2 alone and in complex with CRLR are almost identical, except that, in the CRLR–RAMP2 complex, the C-terminal tail of RAMP2, following Cys131, significantly bends toward CRLR [Fig. 2(C)]. This conformational change is likely to be important for the stable complex formation, because the RAMP2 C-terminal tail, with the bend toward CRLR, exhibits three intermolecular hydrogen bonds and effectively interacts with CRLR (as described in the next section). We noticed a similar conformational change between the structures of RAMP1 alone and in complex with CRLR [Fig. 2(B)].[17]

RAMP2 possesses a hydrophobic patch on α2 and α3, including Tyr93, His124, and Phe128 [Fig. 2(D,E)], and utilizes this patch to interact with CRLR. A similar hydrophobic patch exists in RAMP1,[16] and as we predicted, it contributes to CRLR binding.[17] On the other hand, CRLR possesses a hydrophobic patch on α1 [Supporting Information Fig. S3(A)], for the interaction with RAMP2 as well as RAMP1.

CRLR–RAMP2 interface

RAMP2 α2 and α3 form both hydrophobic and hydrophilic interactions with CRLR α1. As viewed from the N-terminus of CRLR α1 [Fig. 3(A)], a number of hydrophobic interactions are formed by the side chains of RAMP2 Tyr93, Arg97, and Ser94 with CRLR Met42 (α1), RAMP2 Trp86, Phe128, Tyr93, and His124 with CRLR Tyr46 (α1), RAMP2 Ile120, Phe121, and His124 with CRLR Tyr49 (α1), and RAMP2 Phe121, Gln125, and Ala129 with CRLR Met53 (α1). In addition, the main chain of RAMP2 Gly110 forms a hydrophobic interaction with CRLR Arg119 (loop 5). As viewed from the C-terminus of CRLR α1 [Fig. 3(B)], many hydrogen bonds are formed by the side chains of Gly71–Arg97 (loop1–α2), Gln45–Tyr93 (α1–α2), Tyr49–Glu117 (α1–α3), Gln50–His124 (α1–α3), Gln50–Phe128 (α1–α3), Gln50–Ser132 (α1–C-tail), Gln54–Cys131 (α1–C-tail), and Gln54–Ala129 (α1–C-tail), corresponding to CRLR–RAMP2.

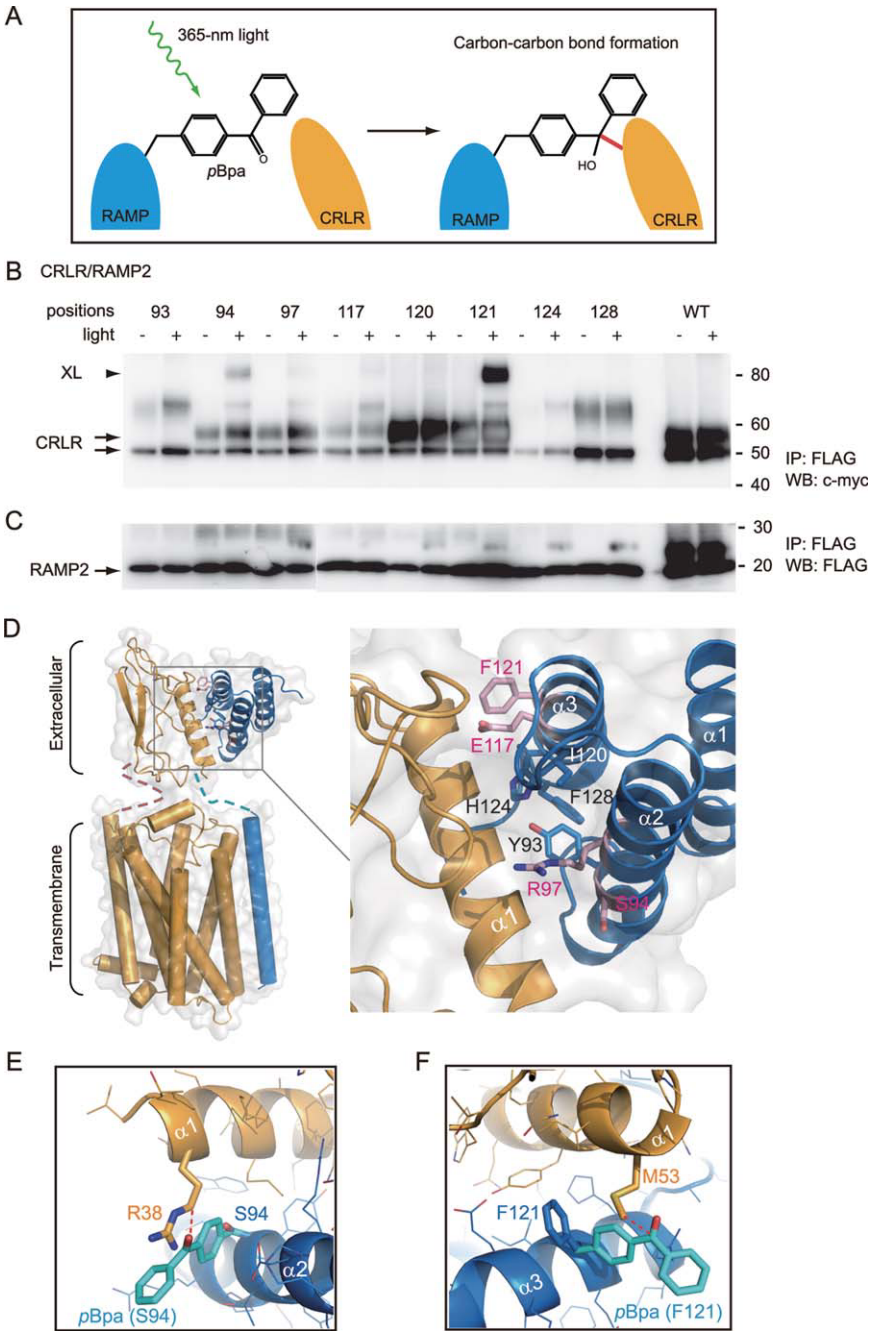

Figure 4. Protein photo-crosslinking of CRLR–RAMP2 in mammalian cells. The FLAG-tagged RAMP2 variants, with the photoreactive amino acid *p*Bpa at the indicated positions, were co-expressed with c-myc-tagged CRLR in HEK293 c-18 cells. After the cells were exposed to light (A), RAMP2 and its photo-crosslinked products were purified by immunoprecipitation with FLAG-M2 agarose. The precipitates were subjected to SDS-PAGE and analyzed by Western blotting with anti-myc (B) and anti-FLAG (C) antibodies. A: Schematic representation of the photo-crosslinking method. B: The uncrosslinked and the crosslinked CRLRs are indicated by the arrows and the arrowhead, respectively. C: The RAMP2 variants are indicated by the arrow. WT: wild type RAMP2; IP: immunoprecipitation; WB: western blotting. D: Structural model for the full-length CRLR–RAMP2 complex, based on the photo-crosslinking results, with close-up views of the interface with the crosslinked amino acid residues. The residues are represented as sticks and are colored pink. E, F: Close-up views of the putative crosslinked locations between *p*Bpa and CRLR.[27]

The deletion of the Trp86–Pro92 region of RAMP2 significantly reduced its cell surface expression.[23] This region corresponds to the N-terminal half of RAMP2 α2, which is involved in the hydrogen-bonding and hydrophobic interactions with CRLR α1. Therefore, the deletion of this region probably disrupts the assembly between CRLR and RAMP2. In addition, the double mutation H124A/H127A of RAMP2 reduced the efficiency of transport to the cell surface and the AM-binding ability of the

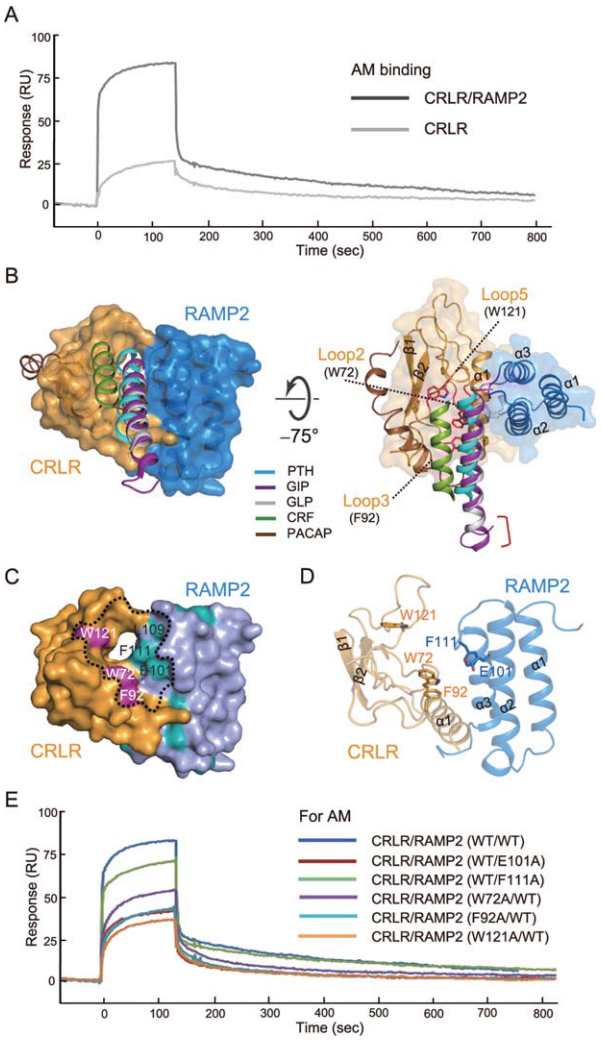

Figure 5. AM-binding affinity and ligand-binding pocket formation of the CRLR–RAMP2 complex. A: Sensorgrams obtained from SPR measurements with the human CRLR–RAMP2 complex and CRLR immobilized on the sensor chip with injections of 1 μ*M* AM. B: The models of hPTH (green ribbon, PDB ID: 3C4M), hGIP (purple ribbon, 2QKH), hExendin-4 (gray ribbon, 3C5T), hCorticoliberin (blue ribbon, 3EHU), and hPACAP (brown ribbon, 2JOD) from their receptor-bound structures were placed on the molecular surface of the CRLR–RAMP2 complex, by superpositioning their receptor structures onto the CRLR structure. The two views are related by a −75° rotation about the horizontal axis. C,D: Molecular surface and cartoon representations of the putative ligand-binding interface of the human CRLR–RAMP2 complex. The dotted area indicates the location of the putative AM-binding region. The cyan surface indicates the locations of identical residues for RAMP2, based on sequence comparisons of RAMP2 and RAMP1 among various species, including human, mouse, bos taurus, and sus scrofa. E: Sensorgrams obtained from SPR measurements with the mutants of the CRLR–RAMP2 complex immobilized on the sensor chip, with injections of 1 μ*M* AM.

AM receptor.[24] This is probably because the mutation of His124 (Fig. 3) to Ala disrupted the CRLR–RAMP2 interface.

Site-specific photo-crosslinking between CRLR and RAMP2 in mammalian cells

We performed experiments with the full-length CRLR and RAMP2 molecules in mammalian cells, to gather evidence to support the determined complex structure of the ECDs. A photo-reactive amino acid, *p*-benzoyl-L-phenylalanine (*p*Bpa), has been site-specifically incorporated into proteins in living cells with an expanded genetic code [Fig. 4(A)].[25,26] This non-natural amino acid is activated by exposure to 365-nm light, and covalently links the *p*Bpa-containing protein and an interacting protein, when the *p*Bpa is incorporated at a site adjacent to the binding interface.[26] To probe the binding mode between the full-length RAMP2 and CRLR molecules, both expressed in human embryonic kidney 293 cells, the crosslinkable amino acid was incorporated into the α2 and α3 helices of RAMP2 at eight separate sites, which interact with CRLR in the determined crystal structure. All eight of these variants were expressed in similar amounts by the cells. Crosslinking detection was performed by Western-blot experiments. RAMP2 and CRLR were C-terminally tagged with FLAG and Myc sequences, respectively, and after exposure of the cells to 365-nm light, the crosslinked products were immunoprecipitated with an anti-FLAG antibody and then detected with an anti-Myc antibody. The molecular masses of the detected complexes were approximately 80 kDa, which is almost equal to the sum of the molecular masses of the two proteins [Fig. 4(B,C)].

The crosslinking patterns of the eight residues of RAMP correspond quite well to the present crystal structure of the extracellular complex. First of all, Ser94 from α2 and Phe121 from α3 are located adjacent to the binding interface, but their side chains are not directly involved in the interaction with CRLR. In fact, the two RAMP2 variants with *p*Bpa at positions 94 and 121 were efficiently crosslinked with CRLR [Fig. 4(D)]. Figure 4(E,F) show possible models of the crosslinking modes[27] in the *p*Bpa94 and *p*Bpa121 variants. On the other hand, Arg97 and Glu117 are close to Ser94 and Phe121, respectively, but are separated by one α helical turn. Thus, Arg97 and Glu117 are located on the edge of the interface, and their side chains hydrogen bond with CRLR. Actually, the *p*Bpa97 and *p*Bpa117 variants also generated the crosslinked products, but with much lower efficiencies than the *p*Bpa94 and *p*Bpa121 variants [Fig. 4(D)]. In contrast, the remaining four residues, Tyr93, Ile120, His124, and Phe128, are located at the center of the interface, and the substitution of the bulky *p*Bpa for these residues is expected to disrupt the CRLR–RAMP2 association. Correspondingly, their *p*Bpa variants failed to generate a crosslinked product. Therefore, the efficient and specific crosslinking of the *p*Bpa94 and *p*Bpa121 variants strongly indicates that the α2 and α3 helices interact with each other on the cell membrane, in the same manner as in the present crystal structure.

Table II. *Summary of SPR Measurements for CRLR and RAMP2/1 Binding to AM and αCGRP*

Surface Plasmon Resonance (SPR)		
	K_D (M)	
Immobilized	For AM	
CRLR/RAMP2 (WT/WT)	6.96×10^{-8}	
CRLR (WT)	1.20×10^{-5}	
CRLR/RAMP2 (WT/E101A)	8.77×10^{-5}	
CRLR/RAMP2 (WT/F111A)	3.36×10^{-7}	
CRLR/RAMP2 (W72A/WT)	1.21×10^{-4}	
CRLR/RAMP2 (F92A/WT)	1.30×10^{-4}	
CRLR/RAMP2 (W121A/WT)	2.04×10^{-4}	
Immobilized	For AM	For αCGRP
CRLR/RAMP2 (WT/WT)	6.96×10^{-8}	1.34×10^{-4}
CRLR/RAMP2 (WT/S94R, R97A, E101W, F111W)	3.57×10^{-3}	1.05×10^{-4}
CRLR/RAMP1 (WT/WT)	1.48×10^{-3}	9.11×10^{-6}

Each K_D value represents the average of at least two independent measurements.

Ligand binding pocket of the AM receptor

We examined the AM-binding ability of the prepared CRLR–RAMP2 complex and CRLR, by surface plasmon resonance (SPR) methods. For this purpose, a synthetic AM peptide was used at five different concentrations, while either CRLR–RAMP2 or CRLR was immobilized on the sensor chip. Under the measurement conditions, the CRLR–RAMP2 and CRLR proteins are expected to be a heterodimer and a monomer, respectively (Supporting Information Fig. S1). The two proteins show clear differences in their ligand-binding affinities [Fig. 5(A)] (Table II). The CRLR extracellular domain itself weakly binds AM, with a dissociation constant (K_D) value of 12.0 μM. In contrast, the AM-binding affinity of the CRLR–RAMP2 complex is 172-fold higher, as compared to that of the CRLR extracellular domain alone, with a K_D value of 69.6 nM. These results provide direct evidence that the RAMP2 and CRLR ECDs coordinately bind AM.

The overall fold of the CRLR extracellular domain resembles those recently determined for other class-B GPCRs, such as GIPR,[13] PAC1R,[28] PTH1R,[11] CRFR1,[29] and GLP1R,[12] in their ligand peptide-bound structures (PDB codes 2QKH, 2JOD, 3C4M, 3EHU, and 3C5T, respectively) [Supporting Information Fig. S3(B,C)]. When these peptide-bound GPCR structures are superposed onto CRLR in the CRLR–RAMP2 complex, the PTH, GIP, and GLP peptides are located close to RAMP2, whereas the CRF and PACAP peptides are far from RAMP2 [Fig. 5(B)]. Therefore, AM is likely to bind to CRLR in a manner similar to those of the PTH/GIP/GLP peptides.

On CRLR, the side chains of three residues, Trp72, Phe92, and Trp121, from loops 2, 3, and 5, respectively, are located on a concave surface, and face RAMP2 [Fig. 5(B,C)]. On the other hand, a comparison of the human, mouse, bovine, and porcine RAMP2 and RAMP1 sequences identified the RAMP2-specific residues [Fig. 5(C)]. Among them, Glu101, Leu109, and Phe111 are located on α2. The side chain of Leu109 is involved in the hydrophobic core, while those of Glu101 and Phe111 are exposed and extended toward CRLR [Fig. 5(D)]. Thus, these exposed CRLR and RAMP2 residues are arrayed within a pocket jointly formed by CRLR and RAMP2 [enclosed by a dashed line in Fig. 5(C)], and are likely to be involved in ligand binding.

To test this hypothesis, we generated mutant RAMP2 and CRLR proteins. Two and three putative ligand-binding residues in RAMP2 (Glu101 and Phe111) and CRLR (Trp72, Phe92, and Trp121), respectively [Fig. 5(D)], were replaced with Ala, and the effect of each mutation on the AM-binding ability of the CRLR–RAMP2 complex was examined by the SPR analysis, as described above [Fig. 5(E)]. The W72A, F92A, and W121A mutations of CRLR caused drastic reductions in the AM-binding affinity (1,740-, 1,870-, and 2,940-fold increases in K_D, respectively) (Table II). On the other hand, the E101A mutation of RAMP2 significantly decreased the AM-binding affinity (1260-fold increase in K_D), while the F111A mutation decreased it modestly (4.83-fold increase in K_D) (Table II). The results indicated the unambiguous roles of these CRLR and RAMP2 residues in AM binding.

Transplanting RAMP1-specific residues into RAMP2

Thus, we showed that the RAMP2-specific residues Glu101 and Phe111 are involved in the AM-binding pocket [Fig. 5(C)]. On the other hand, a comparison of the RAMP1 and RAMP2 sequences from four mammals revealed that the RAMP1-specific residues, Cys82 and Trp84, are located on the RAMP1 α2 helix [Fig. 6(A)]. In the amino acid sequences, the RAMP1-specific Cys82 and Trp84 correspond to the RAMP2-specific Leu109 and Phe111, where Cys82 forms a RAMP1-specific disulfide bond with Cys27. By contrast, human RAMP1 Trp74, corresponding to the RAMP2-specific Glu101, is not conserved in the other three RAMP1 proteins. Like RAMP2, RAMP1 forms a putative ligand-binding pocket along with CRLR, and the RAMP1-specific Trp84 is located at its center. Thus, these RAMP2- and RAMP1-specific residues seem to be responsible for the different ligand-binding specificities between the CGRP and AM receptors. The RAMP2 proteins have the conserved Ser94 and Arg97 residues near the putative ligand-binding pocket, whereas Arg67 and Ala70 are not conserved in the RAMP1 proteins. Thus, we mutated four RAMP2 residues (Ser94, Arg97, Glu101, and Phe111) to the corresponding residues of RAMP1 (Arg, Ala, Trp and Trp, respectively) [Fig. 6(B)], and examined the effects of the mutations on AM and αCGRP binding. The quadruple mutation of RAMP2 (S94R/R97A/E101W/F111W) remarkably

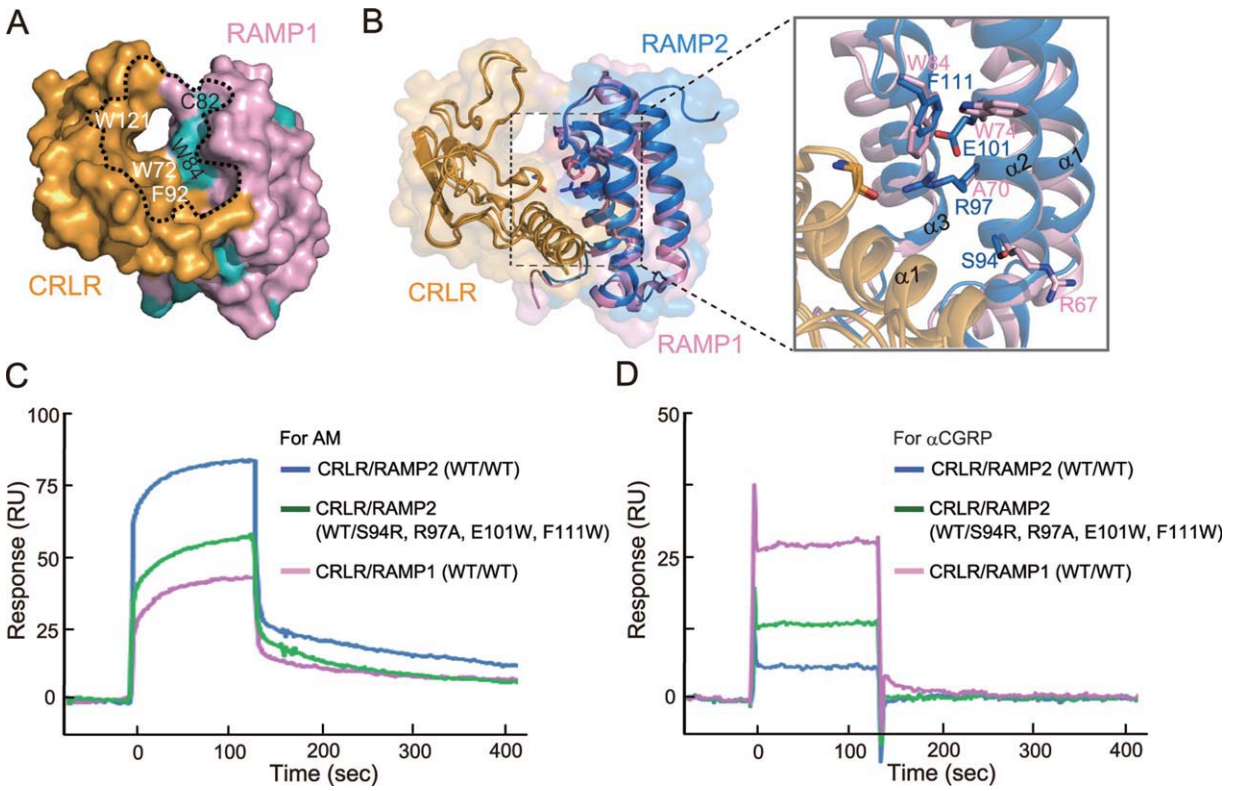

Figure 6. Transplanting RAMP1-specific residues into RAMP2. A: Molecular surface of the putative ligand-binding interface of the human CRLR–RAMP1 complex. The cyan surface indicates the locations of identical residues for RAMP1, and was generated and represented in the same manner as in Figure 5(C). B: Comparison of the amino acid residues between RAMP2 and RAMP1. Close-up view of the putative ligand-binding pocket between CRLR and RAMP2, and CRLR and RAMP1 (right). C,D: Sensorgrams obtained from SPR measurements with the CRLR–RAMP2 complex and the CRLR–RAMP1 complex immobilized on the sensor chip with injections of AM (1 μ*M*) (C), αCGRP (10 μ*M*) (D), respectively.

decreased the binding affinity of the CRLR–RAMP2 complex for AM, as compared to the wild type, and its AM-binding affinity was close to that of the wild-type CRLR–RAMP1 complex [Fig. 6(C)] (Table II). On the other hand, the binding affinity for αCGRP of the CRLR–RAMP2 (S94R/R97A/E101W/F111W) complex was nearly the same as that of the wild-type CRLR–RAMP2 complex, and is therefore much lower than that of the CRLR–RAMP1 complex [Fig. 6(D)] (Table II). Consequently, the transplantation of the four residues of RAMP1 into RAMP2 failed to convert the ligand specificity from AM to αCGRP.

Difference in the pocket shapes between the AM and CGRP receptors

We compared the structures of the CRLR–RAMP2 complex (the AM receptor) and the CRLR–RAMP1 complex (the CGRP receptor), by superimposing the CRLR region. The surface area buried in the CRLR–RAMP1 interface (1010 Å^2) is similar to that in the CRLR–RAMP2 interface (924 Å^2). Interestingly, the putative ligand-binding pocket of the AM receptor is shallower than that of the CGRP receptor; Arg97 (α2), Glu101 (α2), Leu109 (loop2), Phe111 (loop2), and Pro112 (loop2) of RAMP2 are closer to the surface than the corresponding residues of RAMP1 [Fig. 7(A)]. This difference arises because the position of RAMP2 relative to CRLR is rotated and shifted, as compared to that of RAMP1 [Fig. 7(B)], although the RAMP2 and RAMP1 structures themselves are highly superimposable on each other [Fig. 7(C)]. Thus, α2 of RAMP2 is closer to CRLR α1, and conversely, α3 of RAMP2 is farther away from CRLR α1, and thereby alters the shape of the ligand-binding pocket.

Correspondingly, the CRLR–RAMP2 and CRLR–RAMP1 interfaces differ from each other. First, in the RAMP2 α2–CRLR α1 interactions, the RAMP2-specific Arg97 side chain forms an intramolecular salt bridge with Glu101, and hydrogen bonds with the main-chain carbonyl group of CRLR Gly71 [Fig. 7(D)]. In contrast, RAMP1 has Ala70 and Trp74 at the positions corresponding to Arg97 and Glu101 in RAMP2. On the other hand, the RAMP1 Trp59 side chain hydrogen bonds with CRLR Thr43, but the corresponding RAMP2 Trp86 side chain forms hydrophobic interactions [Fig. 7(D)]. The RAMP1 Asp71 side chain forms a salt bridge with CRLR Arg38, whereas the corresponding RAMP2 Asp98 side chain is rotated away. Due to these differences, RAMP2 α2 and RAMP1 α2 are distinctly oriented relative to CRLR α1. Second, in the RAMP2/1 α3–CRLR ξ interactions, CRLR Tyr49 forms hydrophobic interactions with RAMP2 Ile120 and

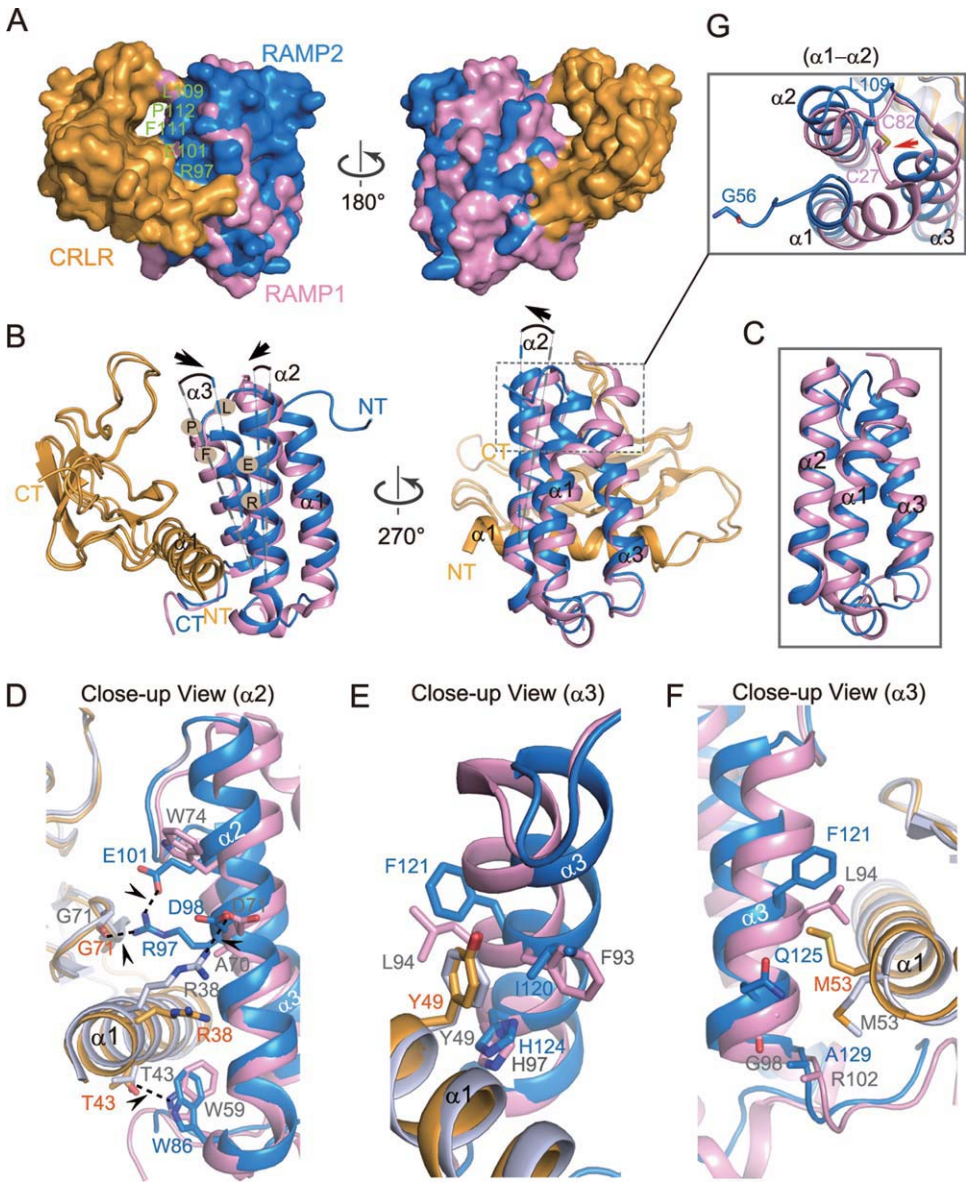

Figure 7. Divergence in CRLR–RAMP heterodimer formation by the AM and CGRP receptors. A,B: Superimposition of the AM and CGRP receptors, based on the CRLR molecule. The two views are related by a rotation about the vertical axis. C: Superimposition of the Cα atoms of the RAMP2 and RAMP1 molecules alone. The views are the same as those on right side of (B). D–F: Close-up views of the CRLR–RAMPs interfaces in the AM and CGRP receptors. G: Superimposition of the Cα atoms of the RAMP2 and RAMP1 molecules in the AM and CGRP receptors.

Phe121, and with RAMP1 Phe93 and Leu94 [Fig. 7(E)]. The main chain of RAMP2 Phe121 is farther away from CRLR than that of RAMP1 Leu94. Nevertheless, the longer Phe121 side chain of RAMP2 and the shorter Leu94 side chain of RAMP1 interact similarly with the CRLR Tyr49 side chain. Correspondingly, the CRLR Met53 side chain adopts distinct orientations between the two complexes [Fig. 7(F)].

In addition, RAMP2 Leu109 is involved in the hydrophobic core, and the corresponding RAMP1 Cys82 forms a disulfide bond with RAMP1 Cys27, corresponding to RAMP2 Gly56. Thus, RAMP2 α1 and RAMP1 α1 are straight and kinked, respectively, which causes significant shifts of the α2 and α3 backbones [Fig. 7(G)]. In this manner, α2 and α3 of RAMP2 are distinctly oriented relative to CRLR, as compared to those of RAMP1, thus causing the different depths and shapes of the ligand-binding pockets between the two receptors.

In conclusion, the distinct ligand specificities of the AM and CGRP receptors are derived from the differences in the side chains and the backbone positions of the ligand-binding pocket residues. Therefore, our transplantation experiment failed to confer RAMP1-like ligand specificity on the CRLR–RAMP2 complex because of the global difference in the relative positions of RAMP2 and RAMP1, in their respective complexes with CRLR.

Materials and Methods

Sample preparation

The DNA fragments encoding the ECDs of human RAMP2 (residues 56–139) and CRLR (residues 23–136) were cloned into the TA vector pCR2.1TOPO (Invitrogen). The RAMP2 and CRLR ECDs were produced as fusion proteins containing an N-terminal histidine tag and a tobacco etch virus (TEV) protease cleavage site. The selenomethionine (SeMet)-labeled proteins were synthesized by the *Escherichia coli* cell-free system, using the large-scale dialysis mode.[30,31] Both the RAMP2 and CRLR ECDs precipitated during synthesis. The precipitated proteins were denatured, and were refolded together (co-refolded) or separately by rapid dilution into 50 m*M* Tris-HCl buffer (pH 8.3), containing 1 *M* arginine hydrochloride, 5 m*M* reduced glutathione, and 0.5 m*M* oxidized glutathione. The co-refolded CRLR–RAMP2 extracellular domain complex and the separately refolded RAMP2 and CRLR ECDs were each purified using a His-Trap column, and then the histidine tags were enzymatically removed with TEV protease. The refolded proteins were further purified to homogeneity by chromatography on anion exchange (Resource Q) and gel filtration (Superdex 200 HR 10/30) columns. All columns were purchased pre-packed from GE Healthcare.

Crystallization and data collection

The preliminary crystals of the SeMet-labeled RAMP2 extracellular domain were obtained by initial crystallization screening, using the 96-well sitting drop vapor diffusion method with 0.5% agarose (Hampton Research). The crystals of RAMP2 used for structure determination were obtained by mixing the protein solution (22.7 mg/mL in 20 m*M* Tris-HCl buffer, pH 7.0, containing 300 m*M* NaCl) with an equal volume of reservoir solution (0.1 *M* sodium-HEPES, pH 7.2, 25% (v/v) PEG400, and 0.2 *M* calcium chloride di-hydrate) and incubating the mixture at 293 K by the hanging drop vapor diffusion method. Plate-like crystals grew to average dimensions of 0.8 mm × 0.3 mm × 0.2 mm within a week.

Diffraction quality crystals of the SeMet-labeled CRLR–RAMP2 complex were grown by mixing the protein solution (8.6 mg/mL in 20 m*M* Tris-HCl buffer, pH 7.0, containing 150 m*M* NaCl) with an equal volume of reservoir solution (0.1 *M* bis-Tris, pH 6.5, 30% (v/v) PEG MME550, 0.05 *M* calcium chloride) and incubating the mixture at 293 K, using the sitting drop vapor diffusion method. Large, single crystals measuring 0.6 mm in the longest dimension appeared within seven to ten days.

Single crystals of RAMP2 and CRLR–RAMP2 were coated with their reservoir solutions, respectively containing 22.5% PEG400 and 20% glycerol as cryoprotectants, mounted using a nylon loop (Hampton Research) and flash-cooled in the cold stream of the goniometer. The diffraction data for the MAD method were collected at 100 K at three different wavelengths at BL26B2, SPring-8, Harima, Japan, and were recorded on a Jupiter210 CCD detector (Rigaku, Tokyo, Japan). All of the diffraction data were processed with the HKL2000 program.[32]

Structure determination and refinement

The program SOLVE[33] was used to locate the SeMet sites and to calculate the initial MAD phases for the RAMP2 and CRLR–RAMP2 data. The program RESOLVE[34] was used for the phase expansion and the density modification. Model building and correction were performed iteratively, using O[35] and COOT,[36] and the structure refinement was performed using Crystallography & NMR system (CNS)[37] and PHENIX.[38] Refinement statistics are presented in Table I and Supporting Information Table S1. The quality of the model was inspected by the program PROCHECK.[39] Most of the graphic figures were created using the program PyMol (DeLano Scientific, Palo Alto, CA). The atomic coordinates and the structure factors have been deposited in the Protein Data Bank, with the accession codes 3AQE and 3AQF.

Acknowledgments

Authors would like to thank N. Shinya, K. Honda, M. Inoue, M. Aoki, T. Yamaguchi, and M. Toyama for experimental assistance. Authors also thank M. Yamamoto for data collection at the RIKEN Structural Genomics beamline BL26B2 at SPring-8. Authors thank the members of the Support Unit for Bio-material Analysis, RIKEN BSI Research Resource Center, for the AM peptide synthesis.

References

1. Kitamura K, Kangawa K, Kawamoto M, Ichiki Y, Nakamura S, Matsuo H, Eto T (1993) Adrenomedullin: a novel hypotensive peptide isolated from human pheochromocytoma. Biochem Biophys Res Commun 192: 553–560.
2. Ichikawa-Shindo Y, Sakurai T, Kamiyoshi A, Kawate H, Iinuma N, Yoshizawa T, Koyama T, Fukuchi J, Iimuro S, Moriyama N, Kawakami H, Murata T, Kangawa K, Nagai R, Shindo T (2008) The GPCR modulator protein RAMP2 is essential for angiogenesis and vascular integrity. J Clin Invest 118:29–39.
3. Iinuma N, Sakurai T, Kamiyoshi A, Ichikawa-Shindo Y, Arai T, Yoshizawa T, Koyama T, Uetake R, Kawate H, Muto SI, Tagawa YI, Miyagawa S, Shindo T (2010) Adrenomedullin in sinusoidal endothelial cells play protective roles against cold injury of liver. Peptides 31: 865–871.
4. Recober A, Kuburas A, Zhang Z, Wemmie JA, Anderson MG, Russo AF (2009) Role of calcitonin gene-related peptide in light-aversive behavior: implications for migraine. J Neurosci 29:8798–8804.
5. Fritz-Six KL, Dunworth WP, Li M, Caron KM (2008). Adrenomedullin signaling is necessary for murine lymphatic vascular development. J Clin Invest 118:40–50.

6. Udawela M, Christopoulos G, Tilakaratne N, Christopoulos A, Albiston A, Sexton PM (2006) Distinct receptor activity-modifying protein domains differentially modulate interaction with calcitonin receptors. Mol Pharmacol 69:1984–1989.
7. Christopoulos A (2002) Allosteric binding sites on cell-surface receptors: novel targets for drug discovery. Nat Rev Drug Discov 1:198–210.
8. McLatchie LM, Fraser NJ, Main MJ, Wise A, Brown J, Thompson N, Solari R, Lee MG, Foord SM (1998) RAMPs regulate the transport and ligand specificity of the calcitonin-receptor-like receptor. Nature 393:333–339.
9. Hoare SR (2005) Mechanisms of peptide and nonpeptide ligand binding to Class B G-protein-coupled receptors. Drug Discov Today 10:417–427.
10. Parthier C, Reedtz-Runge S, Rudolph R, Stubbs MT (2009) Passing the baton in class B GPCRs: peptide hormone activation via helix induction? Trends Biochem Sci 34:303–310.
11. Pioszak AA, Xu HE (2008) Molecular recognition of parathyroid hormone by its G protein-coupled receptor. Proc Natl Acad Sci USA 105:5034–5039.
12. Runge S, Thogersen H, Madsen K, Lau J, Rudolph R (2008) Crystal structure of the ligand-bound glucagon-like peptide-1 receptor extracellular domain. J Biol Chem
13. Parthier C, Kleinschmidt M, Neumann P, Rudolph R, Manhart S, Schlenzig D, Fanghanel J, Rahfeld JU, Demuth HU, Stubbs MT (2007) Crystal structure of the incretin-bound extracellular domain of a G protein-coupled receptor. Proc Natl Acad Sci USA 104: 13942–13947.
14. Hay DL, Poyner DR, Sexton PM (2006) GPCR modulation by RAMPs. Pharmacol Ther 109:173–197.
15. Walker CS, Conner AC, Poyner DR, Hay DL (2010) Regulation of signal transduction by calcitonin gene-related peptide receptors. Trends Pharmacol Sci 31: 476–483.
16. Kusano S, Kukimoto-Niino M, Akasaka R, Toyama M, Terada T, Shirouzu M, Shindo T, Yokoyama S (2008) Crystal structure of the human receptor activity-modifying protein 1 extracellular domain. Protein Sci 17: 1907–1914.
17. ter Haar E, Koth CM, Abdul-Manan N, Swenson L, Coll JT, Lippke JA, Lepre CA, Garcia-Guzman M, Moore JM (2010) Crystal structure of the ectodomain complex of the CGRP receptor, a class-B GPCR, reveals the site of drug antagonism. Structure 18:1083–1093.
18. Gouet P, Courcelle E, Stuart DI, Metoz F (1999) ESPript: analysis of multiple sequence alignments in PostScript. Bioinformatics 15:305–308.
19. Thompson JD, Higgins DG, Gibson TJ (1994) CLUSTAL W: improving the sensitivity of progressive multiple sequence alignment through sequence weighting, position-specific gap penalties and weight matrix choice. Nucleic Acids Res 22:4673–4680.
20. Flahaut M, Rossier BC, Firsov D (2002) Respective roles of calcitonin receptor-like receptor (CRLR) and receptor activity-modifying proteins (RAMP) in cell surface expression of CRLR/RAMP heterodimeric receptors. J Biol Chem 277:14731–14737.
21. Kamitani S, Sakata T (2001) Glycosylation of human CRLR at Asn123 is required for ligand binding and signaling. Biochim Biophys Acta 1539:131–139.
22. Kuwasako K, Kitamura K, Uemura T, Nagoshi Y, Kato J, Eto T (2003) The function of extracellular cysteines in the human adrenomedullin receptor. Hypertens Res 26:S25–S31.
23. Kuwasako K, Kitamura K, Ito K, Uemura T, Yanagita Y, Kato J, Sakata T, Eto T (2001) The seven amino acids of human RAMP2 (86) and RAMP3 (59) are critical for agonist binding to human adrenomedullin receptors. J Biol Chem 276:49459–49465.
24. Kuwasako K, Kitamura K, Nagata S, Kato J (2008) Functions of the extracellular histidine residues of receptor activity-modifying proteins vary within adrenomedullin receptors. Biochem Biophys Res Commun 377:109–113.
25. Chin JW, Cropp TA, Anderson JC, Mukherji M, Zhang Z, Schultz PG (2003) An expanded eukaryotic genetic code. Science 301:964–967.
26. Hino N, Okazaki Y, Kobayashi T, Hayashi A, Sakamoto K, Yokoyama S (2005).Protein photo-cross-linking in mammalian cells by site-specific incorporation of a photoreactive amino acid. Nat Methods 2:201–206.
27. Dorman G, Prestwich GD (1994) Benzophenone photophores in biochemistry. Biochemistry 33:5661–5673.
28. Sun C, Song D, Davis-Taber RA, Barrett LW, Scott VE, Richardson PL, Pereda-Lopez A, Uchic ME, Solomon LR, Lake MR, Walter KA, Hajduk PJ, Olejniczak ET (2007) Solution structure and mutational analysis of pituitary adenylate cyclase-activating polypeptide binding to the extracellular domain of PAC1-RS. Proc Natl Acad Sci USA 104:7875–7880.
29. Pioszak AA, Parker NR, Suino-Powell K, Xu HE (2008) Molecular recognition of corticotropin-releasing factor by its G-protein-coupled receptor CRFR1. J Biol Chem 283:32900–32912.
30. Kigawa T, Yabuki T, Matsuda N, Matsuda T, Nakajima R, Tanaka A, Yokoyama S (2004) Preparation of Escherichia coli cell extract for highly productive cell-free protein expression. J Struct Funct Genomics 5:63–68.
31. Kigawa T, Matsuda T, Yabuki T, Yokoyama S, Bacterial cell-free system for highly efficient protein synthesis. In: Spirin AS and Swartz JR, Eds. (2007) Cell-free protein synthesis. Wiley-VCH, pp 83–97.
32. Otwinowski Z, Minor W (1997) Processing of X-ray diffraction data collected in oscillation mode. Methods Enzymol 276:307–326.
33. Terwilliger TC, Berendzen J (1999) Automated MAD and MIR structure solution. Acta Cryst D55:849–861.
34. Terwilliger TC (2002) Automated structure solution, density modification and model building. Acta Cryst D58:1937–1940.
35. Jones TA, Zou JY, Cowan SW, Kjeldgaard M (1991) Improved methods for building protein models in electron density maps and the location of errors in these models. Acta Cryst A47:110–119.
36. Emsley P, Cowtan K (2004) Coot: model-building tools for molecular graphics. Acta Cryst D60:2126–2132.
37. Brunger AT, Adams PD, Clore GM, DeLano WL, Gros P, Grosse-Kunstleve RW, Jiang JS, Kuszewski J, Nilges M, Pannu NS, Read RJ, Rice LM, Simonson T, Warren GL (1998) Crystallography & NMR system: a new software suite for macromolecular structure determination. Acta Cryst D54:905–921.
38. Adams PD, Afonine PV, Bunkoczi G, Chen VB, Davis IW, Echols N, Headd JJ, Hung LW, Kapral GJ, Grosse-Kunstleve RW, McCoy AJ, Moriarty NW, Oeffner R, Read RJ, Richardson DC, Richardson JS, Terwilliger TC, Zwart PH (2010) PHENIX: a comprehensive Python-based system for macromolecular structure solution. Acta Cryst D 66:213–221.
39. Laskowski RA, MacArthur MW, Moss DS, Thornton JM (1993) PROCHECK: a program to check the stereochemical quality of protein structures. J Appl Cryst 26: 283–291.